What's Wrong With My AIRSAR Data?

David A. Imel*
Jet Propulsion Laboratory 300-243
4800 Oak Grove Drive, Pasadena, CA 91109

AIRSAR Earth Science and Applications Workshop
4–6 March 2002

1 Introduction

AIRSAR data sets can be contaminated with artifacts or glitches: systematic phase or magnitude errors. These artifacts can come from instrument or signal processing, or can be intrinsic to SAR data collection. Some of these errors can be almost completely corrected by post-processing, others cannot, and some are so severe that they can be a cause of data non-delivery. In this paper, I describe each artifact and characterize its impact on the data quality as well as the frequency of its occurrence in AIRSAR data sets.

1.1 Sources of Error

Just about any part of the instrument and processing operation, if not functioning correctly, can lead to artifacts in the data. For example:

Antenna A mis-calibrated antenna pattern, antenna pattern with inadequate side-lobe suppression, or damage to the antenna during the mission. The latter can happen especially during takeoff and landing if there is debris on the runway which can be kicked up by the aircraft tires and shot towards the (exterior) antenna panels.

Cabling An improperly fastened cable can lead to unexpected variations in the antenna pattern, unexpected phase variations during the course of a data acquisition campaign, or even swapped channels. Even with properly fastened cables, the phase delay is temperature sensitive.

Receivers If the gain is set incorrectly, the data may be saturated or buried in the noise. This may happen even for proper gain settings if there is a large variation of the backscatter brightness in the scene being imaged. We use a calibration tone injected into the receiver to monitor gain and phase stability, but extreme changes in gain or phase may not be correctable.

Transmitter Includes both the pulse generators, diode switches, RF multiplier stages and high-power amplifiers (whether solid-state, as in P-band, or travelling-wave tube amplifiers, as in C- and L-band). Typical failures in the past have included a diode switch (used to alternate between top and bottom antennas, vertical and horizontal polarizations, or aft and fore antennas) transmit being shorted to one position. This obviously leads to incorrect interferometric (or polarimetric) signatures. Errors in triggering the pulse generation will introduce phase errors in the transmitted pulses, damaging or making impossible the formation of the synthetic aperture. Damaged (but not completely failed) components in the RF multiplier chain can lead to a loss of bandwidth, and thus a loss of resolution and also incomplete pulse compression (increased ISLR).

Digital System Consisting of the analog-to-digital converters (ADC's), their buffers, and the data

*imel@jpl.nasa.gov

routing and recording system, most of the non-catastrophic errors introduced at this stage can be corrected in software. For example, since the caltone signal is routed through the ADC's (as part of the receiver video output) with a known phase, any mis-triggering of the ADC's is usually correctable by calculating the time shift (in samples) required to alter the observed caltone phase. This is illustrated later in this paper. Errors in the buffer readout can cause the loss of some or all of an entire pulse. But since it takes thousands of pulses to form a synthetic aperture, the loss of any few pulses is usually not noticeable. The data recording system has built-in error correction. If this error correction is overwhelmed, then entire blocks of data can be lost. This is more serious, but is observable during data acquisition. The AIRSAR system acquires data on two recorders simultaneously (one primary, one redundant) to guard against this kind of data loss, as well as later media degredation.

Motion Monitoring System In synthetic aperture radar, the location of the phase center of each antenna must be known precisely in order reconstruct the "synthetic aperture" along a straight reference path. The AIRSAR relies on a Honeywell Embedded GPS / Inertial Navigation Unit (Embedded GPS/INU, or "EGI") to report both the position and attitude of the platform at all times. The lever-arms, fixed in the platform-fixed reference frame, are surveyed initially, then fine-tuned during calibration post-processing. Errors in the position or attitude reported by the EGI translate into defocussing of the SAR image, radiometric errors, and in the case of TOPSAR data, height errors. Moreover, misalignment of the time tagging of this platform state vector and the time tagging of the radar pulses will lead to the same kinds of problems.

Algorithms There are approximations in the signal processing algorithms used to generate the data sets from the raw signal data and telemetry. Some of these approximations break down when the "squint" of the system is too large (i.e., severe cross-winds lead to crabbing of the platform). Other approximations break down when the platform attitude is varying too rapidly, and by too much.

Calibration Errors in calibration can lead to radiometric and height errors. These can be due either to anomalous calibration data sets, or human error. The section on Misregistration in this paper (Section 3.2) describes one such case.

Moreover, there are some kinds of "artifacts" which are not truly errors in either instrument performance or signal processing operations, but are related to the nature of SAR data acquisition. These are also described, in Section 4 of this paper.

2 Instrument Data Glitches

The data artifacts described in this section are caused by incorrect functioning of the instrument hardware. The impact of these kinds of errors ranges from negligible to causing non-delivery of a data set. The artifacts are listed here roughly in order of decreasing severity. Note that some kinds of artifacts may be more severe for certain applications, so that this ordering is not precise.

2.1 DCG Jitter

In order to form a good synthetic aperture, i.e., in order to focus the imagery using the coherent phase of each target as it passes through the radar antenna beam, the exact timing between each pulse must be known. This is accomplished with the AIRSAR instrument by locking both the pulse-transmit and the pulse-recording circuitry to a stable local oscillator (STALO). The frequency stability of the STALO ensures that the phase of each return signal relative to each transmit event, and of one transmit event within a synthetic aperture to any other transmit event, is known.

During the PacRim 2000 data collection campaign, it was occasionally noticed that the timing of the transmit pulses would go out of sync with the recording system, and with each other. The symptom of

this problem would be that the caltone phase for a given channel would cease to be constant. The "caltone" is a single frequency "tone" injected by the pulse generator at the beginning of each receiver chain to monitor the gain and phase stability of the receivers. Since the same tone is injected to more more than one receive chain, if the phase jumps in both receivers by the same amount, it is more likely that the phase jump was caused at the source of the signal, not at both receivers separately but simultaneously. So far as we know, we detected this situation in real-time whenever it occurred, and corrected the problem before acquiring science data. However, if this problem had not been detected and too many pulses had been contaminated with an incorrect transmit phase, it would be difficult or impossible to focus the synthetic aperture image.

An example of this kind of problem is shown in Figure 1, where the phase of the C-band and L-band pulses is occasionally wrong. Note that the C-band and L-band pulses both have the wrong phase at the same time. This eliminates the problem as being that of the digital system or the receivers – it would be too much of a coincidence for two different receive or ADC channels to err on precisely the same pulses. The C-band and L-band radars share the same digital chirp generator (DCG). Thus, when the trigger timing on the DCG is wrong, it affects both the L-band and the C-band data at the same time.

Name:	DCG Jitter
Impact:	Severe, can destroy image
Correction:	Not possible
Occurrence:	None (detected and reflown in real-time)
Reprocessing:	(N/A)

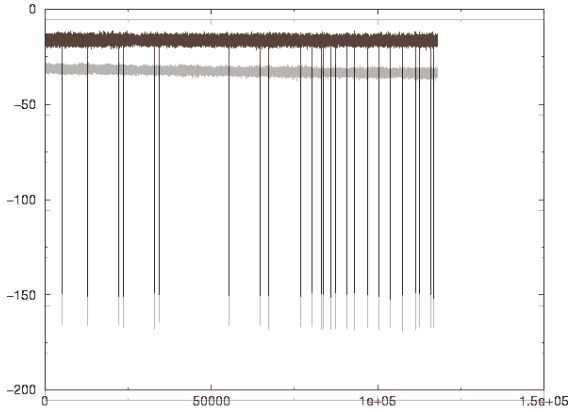

Figure 1: Caltone phase (in degrees) as a function of pulse number. The L-band caltone phase (darker lines) is super-imposed over the C-band caltone phase (lighter lines). The signal for both C- and L-band caltone's is generated by the same digital chirp generator. (P-band uses a separate DCG.) This plot shows a clear signature of a "jittering" chirp-generator.

2.2 LH Receiver Phase Jump

During two of the data lines we acquired during PacRim 2000, we observed a sudden jump in the L-band H-pol channel caltone phase. Since the phase jump occurred only in one channel, we know it was not the caltone signal itself, but the LH receive chain.

Once back in the lab, we were eventually able to reproduce this effect, which is strongly temperature-dependent. On the occasions we observed this during the mission, it seems that the instrument had either been shut down during a long transit and not had sufficient warm-up time, or had been severely "cold-soaked" (in Alaska) the night before the data acquisition flight. The source of the phase jump was eventually isolated to an amplifier, which has been replaced.

Meanwhile, for the data lines with the phase jump, we are processing the data on either side of the phase jump separately, and mosaicking the two pieces together. If this were not done, then the L-band DEM generated from these data (XTI2 mode) would have a large discontinuity in height.

Name:	LH Phase Jump
Impact:	Serious, must divide scene
Correction:	Via mosaicking or new caltone algorithm
Occurrence:	Two datasets (so far)
Reprocessing:	(N/A)

2.3 CV Antenna Pattern Calibration Error

Unique to the Pacific Rim 2000 data acquisition campaign is an anomaly in the antenna pattern in the POLSAR C-band V-pol receive channel. (The anomaly does not appear in TOPSAR data, which uses a different set of antennas and cables.) Dark bands (see Figure 2) appear at particular *look angles* at each pulse along-track in the CVV (i.e., C-band, V-pol transmit, V-pol receive) image. For contrast, Figure 3 shows the same scene's CHH channel image, which does not have this same banding. (There is a small motion-related banding in both scenes which is discussed in subsection 3.4, below.) This banding is most evident over very bright, uniform scenes, such as that of the figures shown, and is more difficult to detect over typical scenes with a variety of vegetation types and topographic features—and also over dark scenes such as the Rosamond calibration site used for the PacRim 2000 calibration.

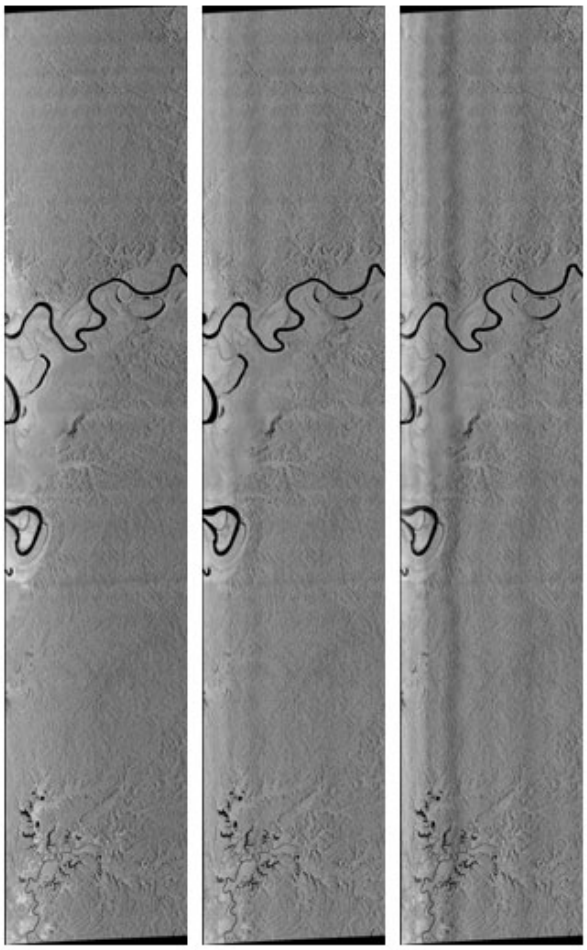

Figure 2: AIRSAR C-band Polarimetric data acquired over Fly River, Papua New Guinea, illustrating the antenna pattern calibration errors. This heavily forested location is an almost uniform scattering scene. From left to right: CHH channel, CVH channel and CVV channel for the uncorrected Fly River scene. The platform flew from the top of the strips to the bottom; slant range increases to the right for these strips. See Figures 4 and 5 for the difference of averaged profiles across these scenes.

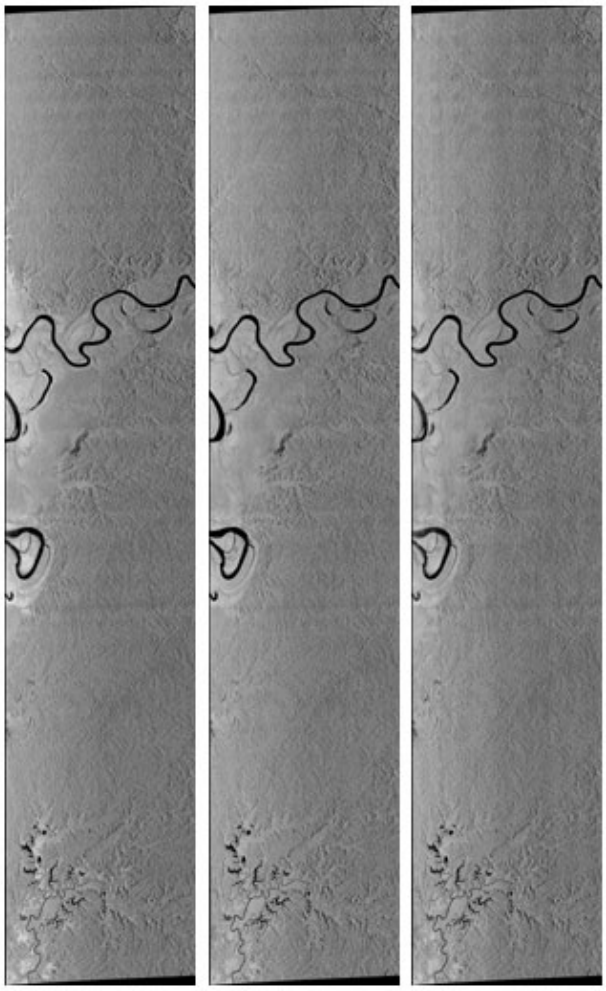

Figure 3: The results of applying the CV-calibration correction to the data of Figure 2 are shown here. From left to right: CHH channel, CVH channel and CVV channel for the corrected Fly River scene. Notice that the vertical banding is much less pronounced for the CVH and CVV channels in these data than that of Figure 2 The platform flew from the top of the strips to the bottom; slant range increases to the right for these strips. See Figures 4 and 5 for the difference of averaged profiles across these scenes.

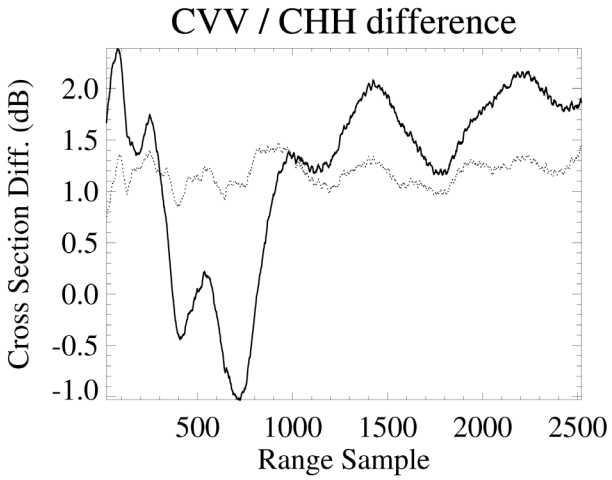

Figure 4: Plot of the CVV/CHH ratio for the Fly River scene (Figures 2 and 3) before (solid curve) and after (dotted curve) correction for the CV-antenna pattern problem.

The C-band POLSAR antenna pattern was measured on the JPL antenna range just prior to the deployment, and no anomalous antenna pattern such as that seen in these data was noted. We believe that there may have been a problem with the cabling between the C-band antenna and the aircraft bulkhead which went undetected during the radar upload and engineering checkout.

We have developed a correction for this anomaly, based on the observation that the anomaly appears to be stable for all of the data sets analyzed for the Pacific Rim 2000 mission, including data sets acquired both at the beginning and the end of the deployment. The size of the anomaly is shown in Figure 4, where the ratio of the CVV-return to that of the CHH-return is averaged over a thousand pulses for a uniform scattering scene. The error introduced into the radiometric calibration by this anomaly (prior to correction) is almost 2 dB. The anomaly has a smaller effect on the CVH channel, i.e., H-pol transmit and V-pol receive, predictably because only one "path" through the CV antenna chain is required for the CVH channel. The same correction curve is applied to correct both CVV and CVH data—in the former

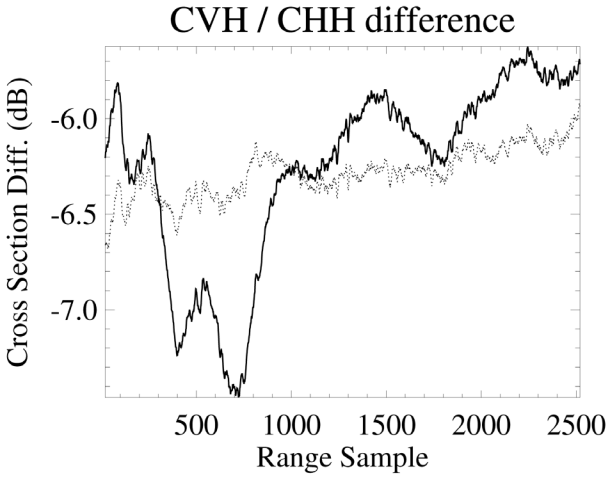

Figure 5: Plot of the CVH/CHH ratio for the Fly River scene (Figures 2 and 3) before (solid curve) and after (dotted curve) correction for the CV-antenna pattern problem.

case, the correction is applied twice.

Starting with version 6.34 of the AIRSAR integrated processor, POLSAR data will be delivered with the CV-anomaly correction applied. Data delivered with earlier versions of the processor do not have the correction applied, but can be re-processed if requested by investigators. The correction is complicated by the fact that the anomaly is a function of look angle which is not accurately known in the case of POLSAR data, since the determination of the look angle requires knowledge of the target location—only obtainable in the TOPSAR mode. POLSAR data are processed using an elevation reference on which all scatterers are assumed to lie. This elevation reference can be used to obtain an approximate look angle, but depending upon the actual topography, the look angle can be incorrect by as much as a few degrees. The implementation of the CV-anomaly correction[1] correlates the observed CVV/CHH ratio against the template correction measured for the mission at every block of 600 pulses in a scene, allowing the location of the match to vary by a few[2] degrees of look angle in order to find the best match.

Name:	CV Pattern Error
Impact:	$\leq$ 2 dB Radiometric Error
Correction:	New correction available
Occurrence:	Every POLSAR data set
Reprocessing:	By request for data from AIPT Version $\leq$ 6.34

2.4 ADC Jitter

Occasionally, our analog-to-digital converters (ADC's) trigger a pulse either one sample late or one sample early, or drop a sample at the beginning of a pulse when the data a read out to data storage. When this happens, the phase of the entire pulse is altered by the missing or extra time corresponding to the number of samples either removed or added, respectively.

We can write that the samples in the frequency domain for a single calibration "tone" are given by:

$$g_j = \sum_{k=0}^{N} f_k e^{2\pi i j k l/N}, \tag{1}$$

i.e., g is the z-transform of f. For the examples in Figure 6 and 7), the sampling frequency is $F_s = 90$ MHz and the calibration tone frequecy $F_c = 43.5$ MHz. A shift by one sample in the time-domain leads to a phase-ramp in the frequency domain, i.e., a change in phase at each frequency sample given by:

$$g'_j = \sum_{k=0}^{N} f_k e^{2\pi i j (k+1) l/N} = e^{2\pi i j/N} g_j. \tag{2}$$

A one-sample shift corresponds to a change in phase at the AIRSAR caltone frequency of $2\pi \times$ (43.5 MHz/90 MHz), or about 174 degrees. An example of this shift is given in Figure 6. Similarly, a

[1] "POLSAR-CV antenna path anomaly in PacRim 2000 deployment", by Yunling Lou, AIRSAR Internal memo. Available on docushare at http://eis-lib.jpl.nasa.gov/eis-lib/dscgi/ds.py/Get/File-16961/CV_ant_anomaly_2000.pdf.

[2] Total variation for the scene, that is. The variation allowed from one patch to the next is much less, to enforce continuity and minimize the possibility of introducing artificial patch boundaries from the correction.

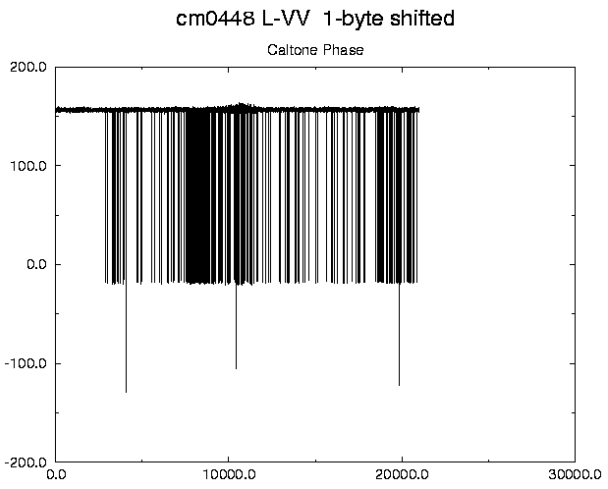

Figure 6: Phase of a single-frequency "caltone" in the L-band VV-pol receive channel. The phase jumps correspond to a shift of one sample. The vertical scale is in degrees of phase and the horizontal scale is pulse number.

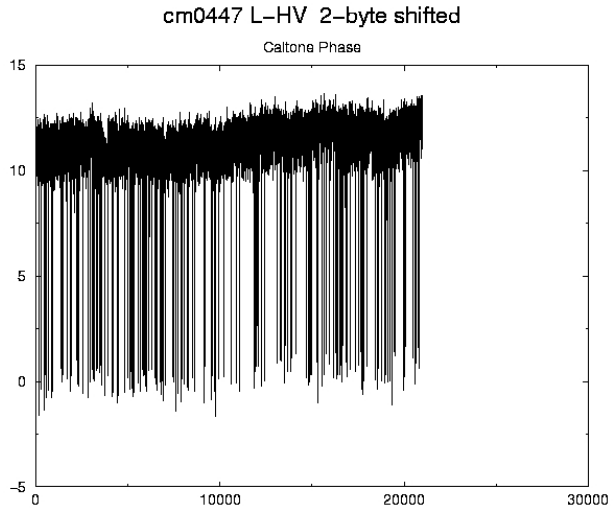

Figure 7: Phase of a single-frequency "caltone" in the L-band HV-pol receive channel. The phase jumps correspond to a shift of two samples. The vertical scale is in degrees of phase and the horizontal scale is pulse number.

two-sample shift corresponds to 348 degrees of phase, which "wraps" to −12 degrees. This is illustrated in Figure 7.

Fortunately, this artifact is pretty well understood (though not well-enough to prevent it from ever happening at the source!), readily detected and easily corrected. Once corrected, it has no impact on our ability to process or deliver data, and also no impact on the data quality.

Name:	ADC Jitter
Impact:	Serious, can defocus image
Correction:	Automated detect/correct
Occurrence:	Occasional
Reprocessing:	(N/A)

2.5 Geo-location Errors

For TOPSAR data, the three-dimensional coordinate of each pixel is given by knowledge of the position vector of the radar platform and antenna phase centers at the time each pixel was imaged as well as the vector from the platform to the pixel. The latter is given for an interferometric SAR by range (from timing the return), azimuth angle (from the Doppler history of the targets in the pixel) and elevation (using the interferometric phase difference). The position vector of the antenna phase centers is obtained for the AIRSAR system with an embedded GPS and inertial navigation unit (INU) system, or EGI, which gives the position of the EGI within the aircraft and monitors the attitude of the platform: roll, pitch and yaw. The lever arms from the EGI to the antenna phase centers are first surveyed, then fine-tuned during calibration.

The EGI has an absolute spherical position accuracy of about 15 meters under nominal conditions. There are some conditions under which the sphere can increase substantially: for example, during PacRim 2000 we observed a loss of GPS lock, and a subsequent worsening of the EGI "Figure of Merit (FOM)" which indicates the absolute position accuracy, when the aircraft would undergo a tight turn, with a roll angle of greater than about 25 degrees.

We tried to avoid this as much as possible. However, data acquisition lines which took us to international borders and occasional redirection by air-traffic control sometimes made these turns unavoidable.

During PacRim 2000, we acquired GPS data with a 12-channel Ashtek receiver, which with one exception during the entire three-month deployment never lost lock. These data are being merged with the EGI position data in the hopes of improving the position accuracy of the combined sensor. Meanwhile, we have also implemented a post-processing geo-location check for each TOPSAR data set. In cases where there is significant geo-location error (i.e., greater than 30 meters), the absolute location of the data are shifted appropriately, re-processed, and the correction confirmed with a final geo-location check. This shift only involves changing the peg-point location (latitude and longitude) in the data headers, and does not involve changing any of the magnitude or phase data.

Name:	Geo-location
Impact:	Significant
Correction:	Straightforward if detected
Occurrence:	Frequent, especially when EGI shows poor FOM
Reprocessing:	By request

2.6 Digital Artifacts in the Raw Signal Data

There are "digital artifacts" which are introduced into the raw signal data from time to time. The most common artifacts are pulses, or parts of pulses, which have been filled in with zeroes instead of the proper byte value corresponding to the voltage observed by the receiver. Other artifacts include short snippets of digital-data. In either case, these artifacts have a byte-value histogram lying far outside the normal histogram of values for the radar scene, and thus have an average power far exceeding the scene. If not corrected, this "digital noise" is multiplied by both the range-compression function and the azimuth reference function during image formation, contaminating a portion of the radar image corresponding to the pulse-duration (in range) and the synthetic aperture (along-track). This is illustrated in Figure 8.

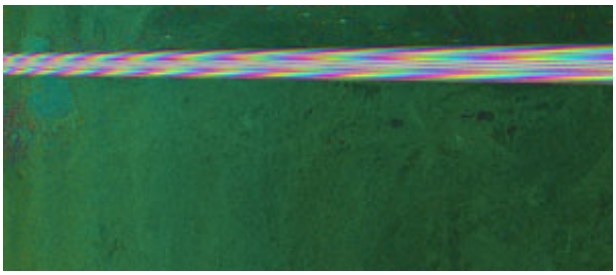

Figure 8: Example of the effect of uncorrected digital artifacts in an AIRSAR C-band along-track interferogram acquired over the Rosamond dry lake bed (the AIRSAR calibration site).

Because the power spectrum of the "digital noise" is different than that of the radar scenery, we have been able to develop a signal processing filter for this noise. At first, we checked pulse-by-pulse with a median filter whose level was set by the brightness in the scene. Any pulse with a significantly larger power than the other pulses within the window of the filter was replaced with a copy of the preceeding pulse. This algorithm was later optimized by tracking the pulse in n separate segments, since the return in the near range is much stronger than that in the far range, and the digital noise was sometimes confined to only one part of the pulse. (The entire pulse is replaced even if only one part of the pulse is contaminated.) We have found that $n = 3$ seems to do an adequate job of eliminating this digital noise. A further refinement would be to replace the pulses (or even, just pulse segments) with random noise of the level appropriate to the radar scene, rather than duplicating the previous pulse. However, at the rates of contamination we observe (0.1% is typical) the difference is not significant.

The contamination does involve loss of information, but has so far been an insignificant fraction of the total data. As long as the digital noise is detected and eliminated, there is no impact of this artifact on data quality.

Name:	Digital Noise
Impact:	Minimal after correction
Correction:	Automated detect/filter
Occurrence:	About 0.1% of all pulses
Reprocessing:	(N/A)

3 Signal Processing Errors

The errors listed in this section come from imperfect signal processing. In some cases, the errors are due to actual bugs in the processing software which have yet to be corrected, in other cases, the errors come from limitations or unwarranted approximations made by the signal processing algorithms. This section also includes calibration errors or uncertainties.

3.1 Phase Bars

An artifact afflicting five of the PacRim 2000 TOPSAR data sets processed so far has been labelled, "phase bars". The problem is not yet completely understood. The symptoms are: small segments (along track) of incorrect interferometric phase which extend across most or all of the slant range. These segments, or bars, occur at patch boundaries. The AIRSAR processor is a "patch processor", meaning that the range-compressed data are brought into a buffer a certain number of along-track pulses at a time, e.g., at least twice the longest synthetic aperture length used, and azimuth compression is performed on the data in the buffer. A portion of the resulting image in the buffer (a patch) is written out, and the buffer is re-filled with new data for the next patch. The patches are then joined together to make the full single-look complex SAR image.

We have found that we can reduce, or even eliminate, these "patch bars" by decreasing the azimuth reference length used for azimuth compression. This is the same procedure used to decrease the impact of azimuth ambiguities. The decreased azimuth reference length means that the intrinsic azimuth resolution is worsened. Obviously, this interim "fix" is not satisfying. It sems likely that there is some sort of software problem in the azimuth compression module of the processor having to do with array bounds being exceeded. Our initial investigations have not been successful in pinning down the source of this problem, but we are still working on it. Figures 9 and 10 illustrate the problem and the workaround, respectively.

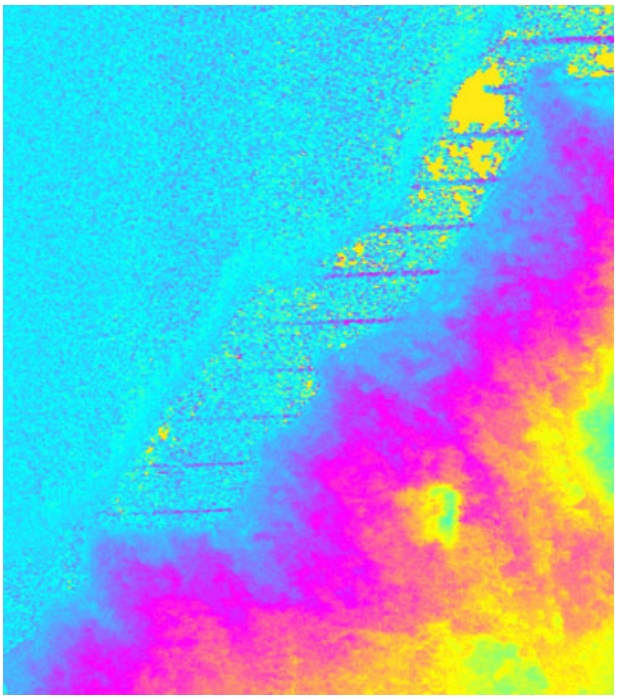

Figure 9: Portion of a C-band DEM showing the coast of West Samoa. The "phase bars" are the horizontal streaks of phase which are most visible as they extend off of the coast. These bars actually extend all the way across the land in this scene, but are difficult to make out visually over land. Here, the platform is moving from top to bottom of the scene, and the range increases to the right.

Name:	Phase Bars
Impact:	Small
Correction:	By decreasing az. res.
Occurrence:	Two datasets so far
Reprocessing:	(N/A)

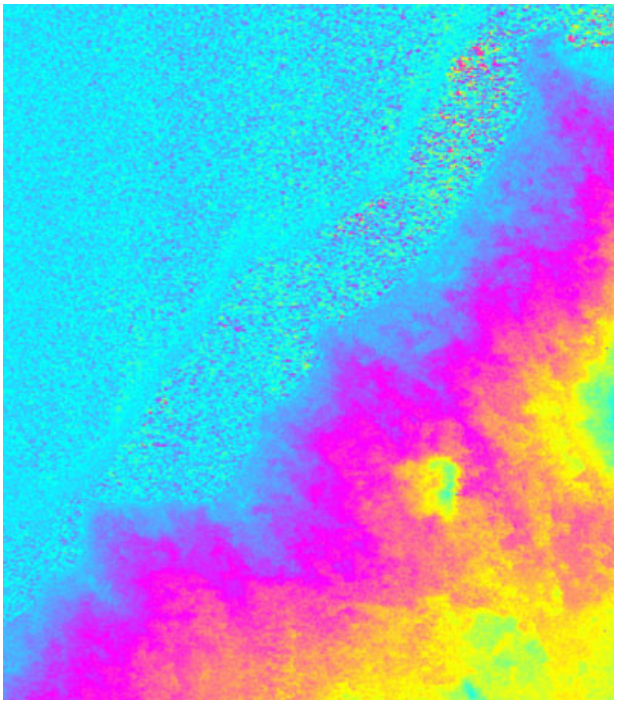

Figure 10: The same scene as Figure 9, where the azimuth bandwidth has been reduced, worsening the azimuth resolution but also greatly reducing the "phase bar" contamination.

3.2 Misregistration

An error in the range-delay for the L-band and P-band 40 MHz data calibration led to a inter-frequency co-registration error: in pre-corrected 40 MHz POLSAR data, there is a slant range offset between the C-band and L-band data sets of about 1 pixel, and between C-band and P-band, 4 pixels. The PacRim 2000 40 MHz POLSAR data sets were easily corrected by applying the appropriate shift in the slant range.

This error also affected TOPSAR data sets. However, in this case, the correction is more complicated. Because the error was made in the slant-range, the offset projected onto the ground for TOPSAR data is not a constant shift. Thus, the P-band data (for XTI2 and XTI2P acquisition modes) and both L-band and P-band data (for XTI1 and XTI1P acquisition modes) had to be re-processed with the correction to the slant range and then re-projected onto the ground. In the process, we discovered that there was often a small misregistration error for TOPSAR data even after the proper slant-range calibration had been made. This is probably due to limitations in the accuracy of the motion-compensation correction. Since the L-band, P-band and C-band antennas are all located in different places on the fuselage, any motion-compensation approximation can affect the three radars differently, leading to a misregistration among them.

In order to ensure that all TOPSAR data are correctly registered, an automated co-registration program[3] is now used to detect TOPSAR misregistration between radar bands in the slant-range intermediate products, apply any necessary range-correction to all of the P-band (and L-band in the case of XTI1 and XTI1P) data, reprocess and re-check the registration.

The re-processing and re-delivery of data sets affected by the misregistration error is now complete. All data sets are now automatically checked to detect any possible multi-frequency registration error.

[3]Built on Scott Hensley's ubiquitous "magcor" program, which finds the appropriate shift between two real-valued images.

Name:	Misregistration
Impact:	L-band: 1 pixel
	P-band: 4 pixels
Correction:	Automated detect/correct
Occurrence:	$\leq$ 6.32 AIPT Version
Reprocessing:	Completed

3.3 Patch-boundaries

As described in Section 3.1, the AIRSAR Integrated Processor (AIPT) is a patch-based processing system. This has the advantage that it can handle larger sections of data than can fit in memory all at once, but has the disadvantage that these patches have to be sewn together to form the final image. The patch boundaries are typically not completely seemless. This can be due to many factors. For example, during image formation, the squint (i.e., the doppler centroid determined by the yaw and pitch of the platform) is determined for each patch and used to determine the look angle and, for TOPSAR data, the baseline. If the platform attitude is varying rapidly, then the approximation that the attitude is constant during a synthetic aperture will fail. This is illustrated in Figure 11, where the height corresponding to a full color-wrap is greatly exaggerated in order to display the patch boundary discontinuities. The discontinuities are quantified in Figure 12, and show that in this case their magnitude can be as large as 1 meter across the patch transition. Obviously, these are only noticeable in very flat terrain, which is why this Angkor, Cambodia scene was chosen to highlight the artifact.

At the Jet Propulsion Laboratory, new processing technology is becoming available[4] which may allow a reduction in the magnitude of the patch-boundary discontinuities.

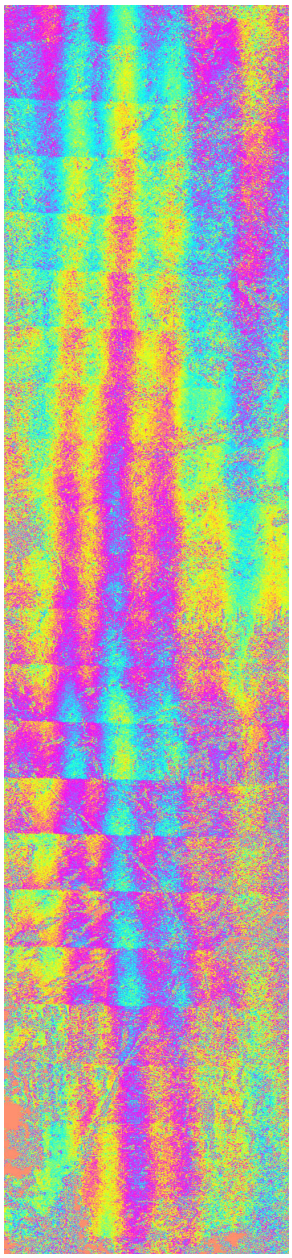

Figure 11: Patch Boundary Discontinuities in the Angkor, Cambodia C-band digital elevation model. Here, the height wrap has been increased to 5 meters in order to highlight the artifacts. The artifacts are the roughly horizontal discontinuities in the color coding of the image. (The multipath effects are the seen as well as the smoothly-varying vertical bands.)

[4] *Improved Processing for AIRSAR Data Based on the GeoSAR Processor*, by Scott Hensley, Elaine Chapin, and Thierry Michel, elsewhere in this workshop proceedings.

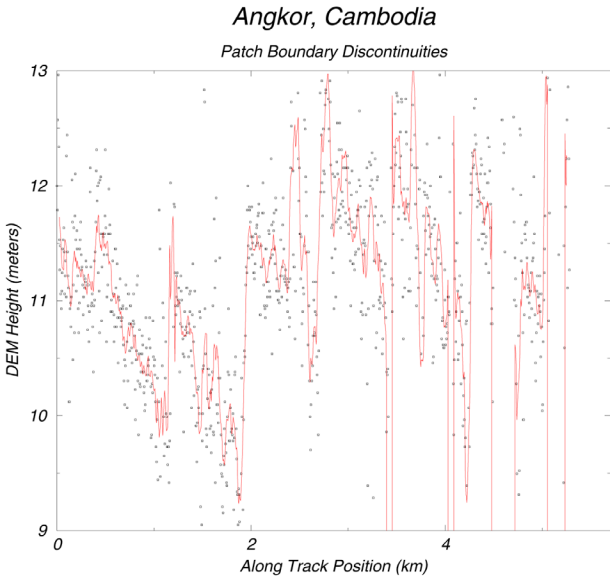

Figure 12: Vertical cut through the C-band DEM of Figure 11. The red curve is a smoothed version, highlighting the size of the patch boundary discontinuities.

Name:	Patch boundaries
Impact:	Minor height errors
Correction:	Not available
Occurrence:	TOPSAR data
Reprocessing:	No

3.4 Motion Compensation Errors

Motion-compensation errors can arise from either errors in the knowledge of the aircraft position and attitude, (necessary) approximations in the motion-compensation correction algorithms, or platform motion that varies too rapidly. In the latter case, just as in the section above, the assumption that the squint for each patch is constant breaks down, and a radiometric error can be introduced. An example of this situation is plotted in Figure 13, where an average across all ranges has been calculated for the very uniform scatterer brightness Fly River scene shown in Figure 2, and the mean subtracted, for each point

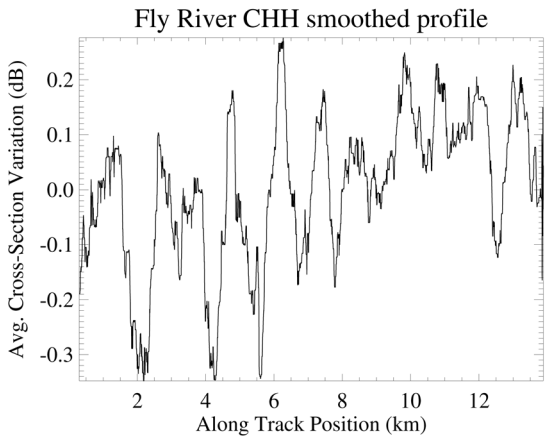

Figure 13: Vertical profile through the CHH scene of Figure 2, showing the amplitude variation due to imperfect compensation for position of the antenna phase centers as the platform's position and attitude varies from a perfect "reference path".

along-track. The undulating variations are due not to intrinsic scatter brightness variations but are due to calibration errors introduced by the breakdown of the signal processing algorithm's ability to deal with a rapidly-varying platform attitude. The cross-section errors can be seen to be as much as 0.5 dB peak-to-peak in this case.

Name:	Mocomp Errors
Impact:	$\leq$ 0.5 dB radiometric errors
Correction:	Not currently available
Occurrence:	During severe platform motion
Reprocessing:	(N/A)

3.5 Annotation Errors

These kinds of errors are not data artifacts in that they do not actually affect data quality. However, for some kinds of analyses by investigators, incorrect data annotation can lead to incorrect analysis. The most recent error of this sort occurred when we expanded the potential number of range samples in

an output image. The radiometric correction vector, which is included in the header data had a hard-coded length (version 6.31 of the processor). We corrected this problem to provide the full radiometric correction vector (version 6.32) but then found that some commercial software used for AIRSAR data analysis (ENVI) assumed the radiometric correction vector length, and actually crashed when fed data wih the proper vector embedded in the header. Therefore we returned the correction vector to its previous length but also wrote a separate file with the full correction vector (version 6.33). None of this had any effect on the polarimetric data themselves, but could affect certain kinds of post-processing analysis of the data.

Name:	Annotation Errors
Impact:	Post-procesing analyses
Correction:	Separate files provided
Occurrence:	All data sets
Reprocessing:	(N/A)

4 Intrinsic Artifacts

These contaminants to AIRSAR data sets come from the nature of SAR itself or from the environment in which the data are acquired. They are not truly "errors", in the sense that the instrument and the signal processing algorithms may be working perfectly, and the data will still have these kinds of artifacts.

4.1 Radio-Frequency Interference

AIRSAR P-band data is especially susceptible to radio-frequency interference (RFI) from airport radars and various kinds of telecommunications, usually associated with urban environments. An example of this kind of interference can be found in Figure 14, where the P-band total power is display in red, LVV in green and CVV in blue. The RFI shows up as red streaks at particular along-track (slow-time) coordinates.

Typically, the RFI contamination appears to be more prominent in the far range. This is due to the way the SAR processor interprets the data: for any

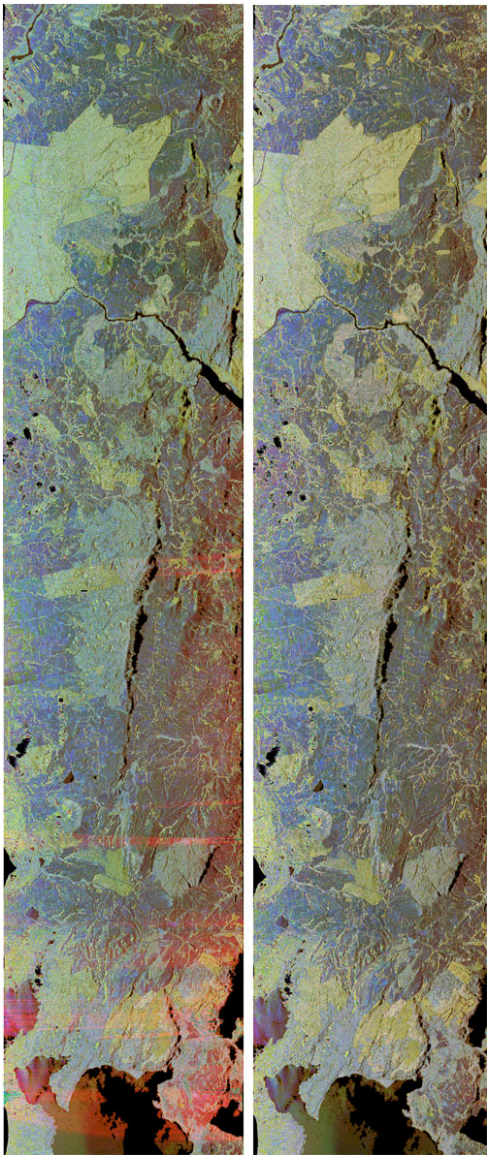

Figure 14: Example of a dataset (Rotorua, NZ) with P-band RFI contamination. Range increases towards the right in both images, while the platform is travelling from top to bottom. Total P-band power is in red, CVV in blue and LVV in green. On the left is the data set before RFI filtering and on the right, after. The red-streaks on the left are the clear RFI signature in this scene.

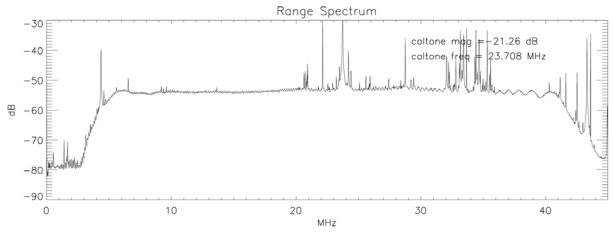

Figure 15: Spectrum for p-band VV-pol channel in the Rotorua, New Zealand scene. Even after filtering to remove radio-frequency interference, there is significant residual contamination in the frequency spectrum which is not, however, evident in the imagery.

given pulse, signals at earlier times are assumed to come from a nearer range, while later times correspond to the farther range in the data swath. Thus, when the range correction is applied, signals from farther away are amplified to compensate for the $1/r^3$ losses. However, the timing of the RFI signals is usually not[5] correlated with the pulse timing. This means that the RFI signals which happen to fall into the far range are amplified by the SAR processor much more than signals which fall into the near range.

In order to compensate for radio-frequency interference, we have incorporated the algorithm developed by Scott Hensley and Charles Le[6] The more recent versions of this filter can go a long way towards reducing (though not eliminating, see Figure 15) the RFI-contamination in the scenes, with relatively small impact to the overall calibration. Nevertheless, there is usually some small overall change in the relative brightness of the different P-band polarimetric channels, as can be seen in Figures 16–18. Therefore, when the RFI-filter is applied, we deliver both the filtered and the unfiltered data sets.

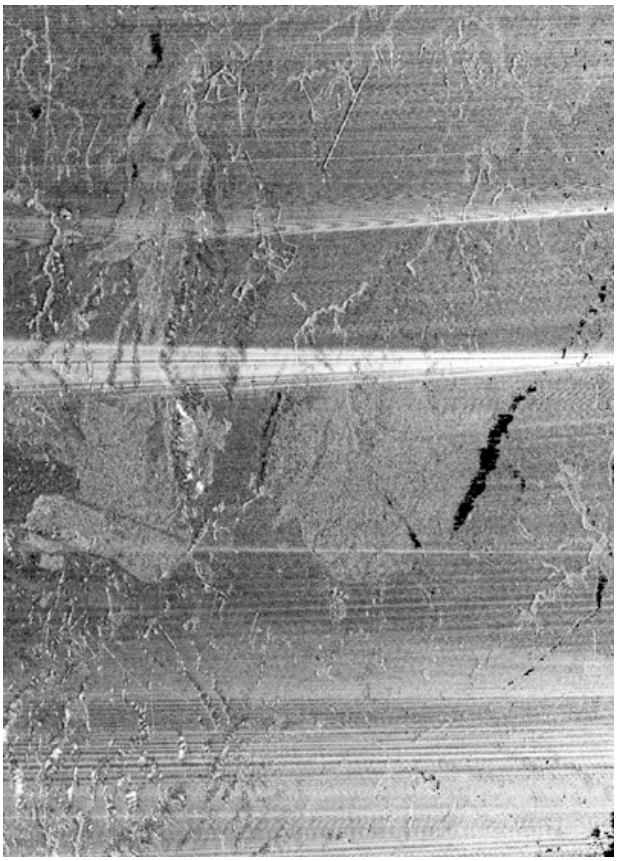

Figure 16: The original PVV image from a data set collected over Rotorua, New Zealand, during the Pacific Rim 2000 campaign. Radio-frequency contamination can be seen as approximately horizontal bright streaks across the image.

[5] We have occasionally observed a "lock-on" by radar installations, in which case the timing can be quite correlated.

[6] *RFI Removal from AIRSAR Polarimetric Data*, by Charles Le and Scott Hensley, elsewhere in the proceedings of this workshop.

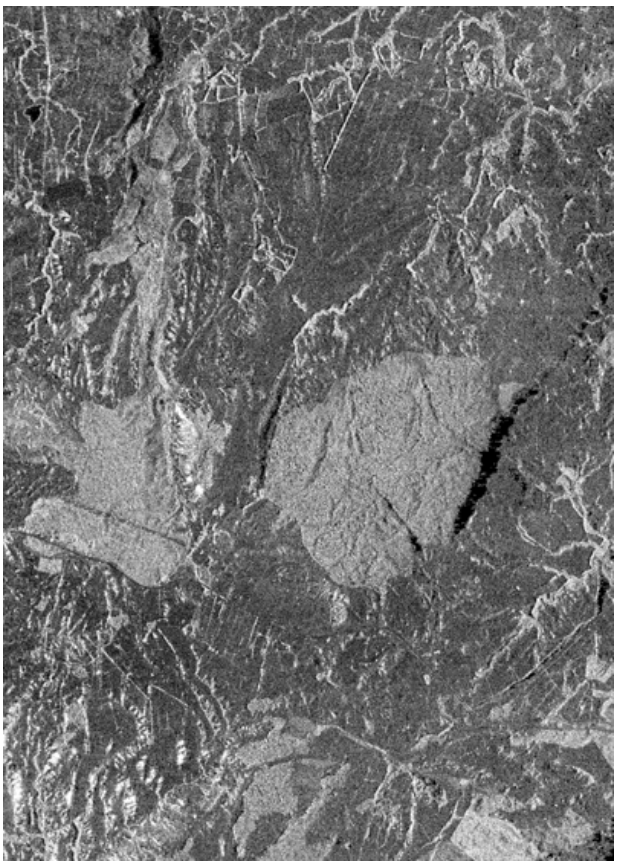

Figure 17: The PVV image of Figure 16, after filtering for RFI. In this case, the RFI removal has done a good job of removing most of the visual contamination, but may have changed the overall calibration—See Figure 18.

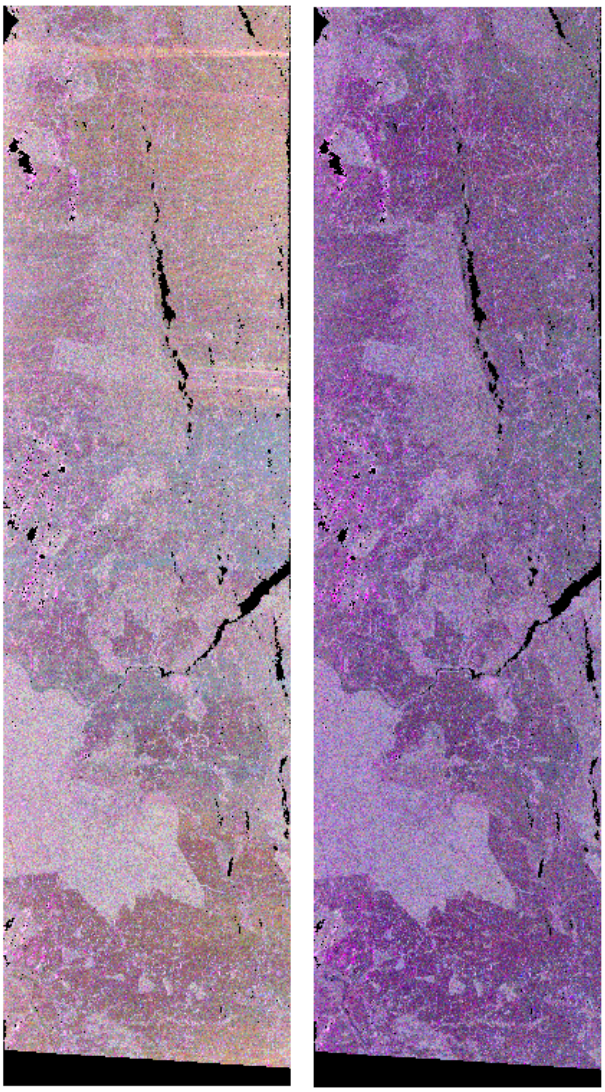

Figure 18: P-band polarimetric image for the Rotorua, New Zealand scene: PVV brightness is in red, PHV in green, and PHH in blue. On the left is the original image, and on the right, the image after RFI-filtering. The filtering has removed most of the obvious contamination, but has also changed the overall ratio of PVV to PHH in the scene.

Name:	RFI
Impact:	Usually P-band only; can destroy P-band cal.
Correction:	Via RFI-filtering
Occurrence:	Near populated areas and airports
Reprocessing:	(N/A)

4.2 Multi-path

When TOPSAR data are acquired, the phase difference between the top and bottom antennas of the interferometric pair are used to calculate the elevation angle of the scattering center in each pixel. The baseline at each point along the platform's path is reconstructed, given the record of the platform attitude and knowledge of the antenna phase center positions in the platform-fixed coordinate system. The interferometric phase is due to the difference in the paths between the pixel scattering center and each antenna phase center:

$$\Phi = 2\pi d/\lambda, \tag{3}$$

where d is the path difference, λ is the radar wavelength and Φ is the interferometric phase. In the absence of contamination by multipath or switch leakage, this path difference is:

$$d = p\mathbf{n} \cdot \mathbf{B} \tag{4}$$

where $\mathbf{n}$ is a unit vector in the look direction from the radar to the pixel, $\mathbf{B}$ is the vector from one antenna phase center to the other (the "baseline vector"), $p = 1$ for "common-transmitter" mode where only one antenna is used to transmit, and $p = 2$ (so-called "baseline doubling") for "ping-pong" mode where transmit alternates from each antenna.

Now, if a multi-path signal is present, say from signals returning from the scattering scene which bounce off of a wing or an engine before arriving at the receive antenna, then some fraction of the signal will be present with an interferometric phase corresponding to

$$d' = \mathbf{n} \cdot \mathbf{B}' + l_m \tag{5}$$

where d' is the path length travelled by the multipath signal, $\mathbf{B}'$ is the baseline between the transmit antenna and the source of the multipath (wing or engine) and l_m is the distance between the multipath source and the receive antenna. To compute the phase actually measured by the system, one would have to sum over all such possible paths, scaling the contributions by the relative scattering cross sections of each source of multipath. This is a difficult problem, and one not attempted here.

Nevertheless, the result of having a signal contribution from a baseline other than the expected one is that there will be height variations with range not corresponding to the scattering topography.

Figures 19–21 illustrate this effect as observed in a data set acquired over Angkor, Cambodia. This area is especially good for highlighting multipath errors because it is very flat. In Figure 21, the effect was quantified by taking the first few kilometers of the scene, making a horizontal slice through the DEM, subtracting the mean elevation, and averaging this operation along-track. The multipath errors here vary from close to zero to as much as ± 3 meters.

We are examining whether or not this multipath pattern is stable over the course of a deployment. It may be only a function of look angle. If so, it may be possible to apply a correction to reduce this source of error. However, it could conceivably be a function of more complicated variables such as fuel loading of the aircraft, altitude and airspeed, in which case an accurate correction will be very difficult.

Name:	Multipath
Impact:	Small height errors
Correction:	Not available yet
Occurrence:	All TOPSAR data, but impacts flat areas most
Reprocessing:	(N/A)

4.3 Unwrapping Problems

The interferometric phase is only observed modulo 2π. The process of phase-unwrapping allows the reconstruction of the absolute phase difference[7] and

[7]—to within one global ambiguous number of of 2π's, which can be obtained if any single height in the scene is known.

Figure 19: Multipath effects on a TOPSAR C-band digital elevation model (DEM). The purple, roughly vertical bands, or fingers extending from the bottom of the scene towards the top, are the multipath height errors in this scene. They show up most clearly in very flat areas, such as the top of this scene, and disappear (visually) in significant relief, such as near the bottom. A full color wrap in this image corresponds to 100 meters of height variation.

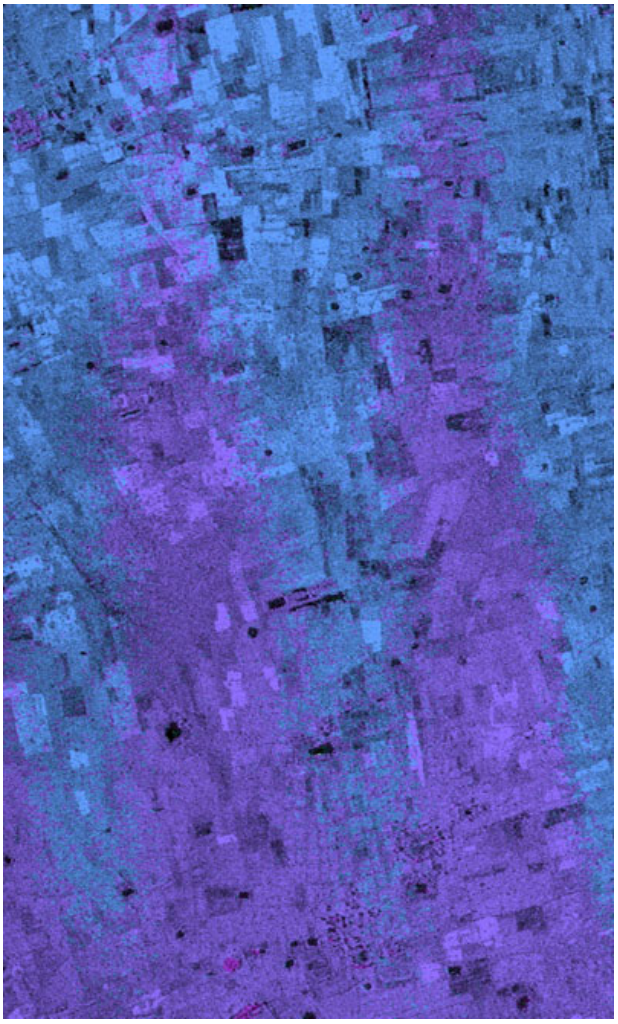

Figure 20: Detail of the upper part of the scene shown in Figure 19 in the region where the plot in Figure 21 has been generated. The alternating bands of purple and blue, corresponding to a meter or two of topography, are due not to the terrain, which is flat, but to multipath contamination of the interferometric phase.

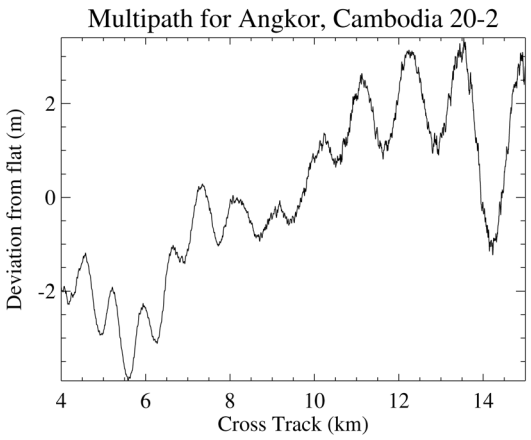

Figure 21: Example of the effect of uncorrected digital artifacts in an AIRSAR data set acquired over Rosamond dry lake bed (the AIRSAR calibration site).

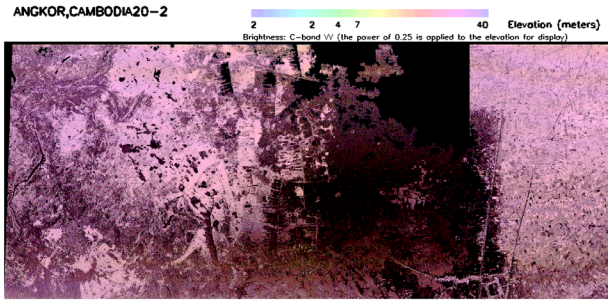

Figure 22: There was significant difficulty in phase-unwrapping the Angkor, Cambodia C-band interferogram used to generate this DEM. The areas which could not be unwrapped are black in this image, where color corresponds to height and brightness corresponds to the backscatter cross-section. The areas which could not be unwrapped had a very low scattering cross-section, but also appear to have occurred along a patch boundary, implying that a systematic phase error may have helped to cause this phase unwrapping failure.

therefore the path difference required to generate a DEM. However, the phase-unwrapping process can be hindered in certain areas where the phase doesn't correspond accurately to the terrain. This can come from shadowing (in areas of significant topographic relief) where the signal from one scatterer is blocked by nearer scatterers, or from areas which are very dark at radar wavelengths (i.e., very smooth) and do not scatter much signal back to the receive antennas. This results in poor signal-to-noise, a low correlation value and a large phase uncertainty, which can foil phase unwrapping programs. In fact, the phase-unwrappers employed by the AIRSAR processor use a "correlation threshhold", below which phase-unwrapping is not even attempted. Phase unwrapping errors can also occur where there are systematic phase errors, such as along patch boundaries (see Subsection patch-boundaries, above). An example of a scene with a significant portion of the data lost to an unwrapping failure is shown in Figure 22. In this case, there may be a combination of the effects just described: the scattering cross section in this flooded area is very low, and thus so is the interferometric correlation. However, the failure to unwrap the phase along what appears to be a patch boundary, with at least part of the scene appearing to have adequate brightness, implies that there may be a systematic phase error fooling the unwrapper at this location. This case is still under study by the AIRSAR processing team.

Name:	Unwrapping Failure
Impact:	Severe—no data available
Correction:	Tweaking of unwrapping algorithm parameters
Occurrence:	Low cross-section scenery
Reprocessing:	(N/A)

4.4 Azimuth Ambiguities

Azimuth ambiguities are a natural outcome of SAR data acquisition and processing arising from a finite pulse-repetition frequency and sidelobes to the azimuth antenna pattern. They occur in AIRSAR data as in any other kind of SAR data, but are only evident in scenes of significant along-track contrast. A good example would be a coastal city, especially if the radar is flown along a direction such that the

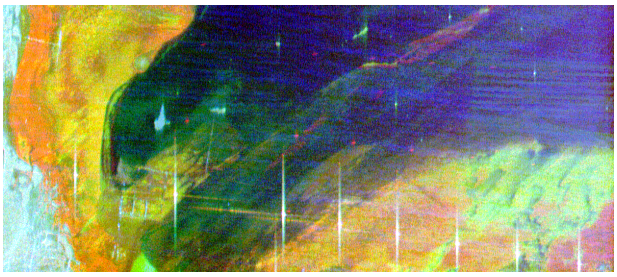

Figure 23: Multi-frequency polarimetric data collected over the AIRSAR calibration site at Rosamond dry lake bed: P-band total power is in red, L-band in green and C-band in blue. The bright targets with large side-lobes distributed in a line from the left lower-center to the lower-right corner are corner reflectors. The small red dots located about one-quarter of the scene above and just to the right of each corner reflector are azimuth ambiguous corner-reflector responses.

sidelobes image the city perpendicular to the streets in the city, giving rise to very bright "double-bounce" returns for the side-lobes. An example of this is shown in Figure 24 at the beginning of the data line over Mt. Fuji, Japan. Azimuth ambiguities can usually be reduced by decreasing the azimuth reference function (the synthetic aperture) used to form the image. However, this also means worsening the azimuth resolution of the data. Typically, if we feel it is necessary to reduce the azimuth resolution, both before- and after-reduction sets of data are delivered.

Name:	Azimuth Ambiguities
Impact:	"ghost images" (−13 to −20 dB)
Correction:	Reduce azimuth resolution
Occurrence:	High contrast areas (coastline)
Reprocessing:	By request

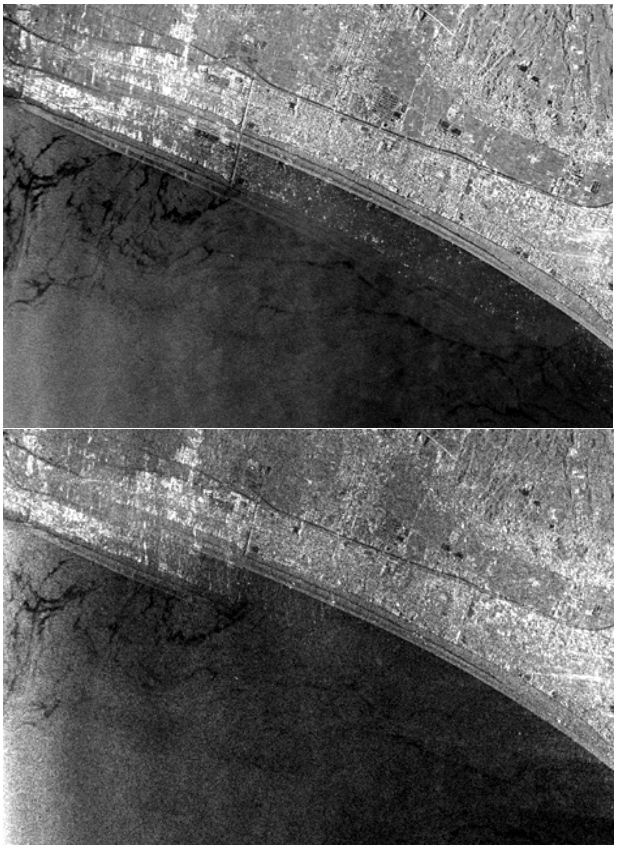

Figure 24: Coastal scene (MtFuji180-1) displaying particularly severe effects of azimuth ambiguity noise as the first sidelobe of the C-band azimuth antenna pattern lines up perpendicular to the city streets along a section of the curving coastline. The upper image shows the azimuth ambiguities and noise at the normal processing resolution. In the lower image, the azimuth bandwidth has been reduced by 40%. The degradation in azimuth resolution is apparent, as well as some reduction in the azimuth ambiguity noise.

4.5 Cross-Talk Removal Failure

One of the steps in the AIRSAR polarimetric processor is "cross-talk removal", where compensation[8] for any polarimetric leakage is applied to the cross-polarized channels. For each polarimetric scene acquired, a single correction which is a function of range only is applied. However, this correction relies on some minimal signal-to-noise ratio (SNR) in order to function correctly. In situations where the SNR is poor at a particular range everywhere along-track, the cross-talk removal algorithm can be fooled. (Basically, there is no true cross-polarization signal—only noise remains in the data for these cases.) Such a case is shown in Figure 25, where the near-range is ocean everywhere in the scene, and the correction is in error. In cases like these, operator intervention is required to avoid making the correction over the specific low-SNR areas.

Name:	Cross-Talk Removal
Impact:	Local radiometric cal. errors
Correction:	"by hand"
Occurrence:	Mixed ocean/land scenes
Reprocessing:	By request

4.6 Uncompensated Topography

In along-track interferometry (ATI) data, the phase is interpreted as motion in of the scatterers in each pixel, rather than topography. But in fact, since the along-track baseline usually includes at least a small cross-track component, any topography in the scene will lead to a phase signature even for stationary scatterers. This phase signature arises in the context of motion compensation, where a constant elevation reference is used in order to correct the phases received at the actual antenna phase centers to those which would have been received at the reference track. In order to make this correction, the location of the scatterers must be assumed; therefore a reference elevation is chosen. In general, for ATI data, sea-level is

[8] "Calibration of Polarimetric Radar Images Using Only Image Parameters and Trihedral Corner Reflectors", by Jakob J. Van Zyl, *IEEE Transactions on Geoscience and Remote Sensing*, **28**, No. 3, May 1990, pp. 337–348.

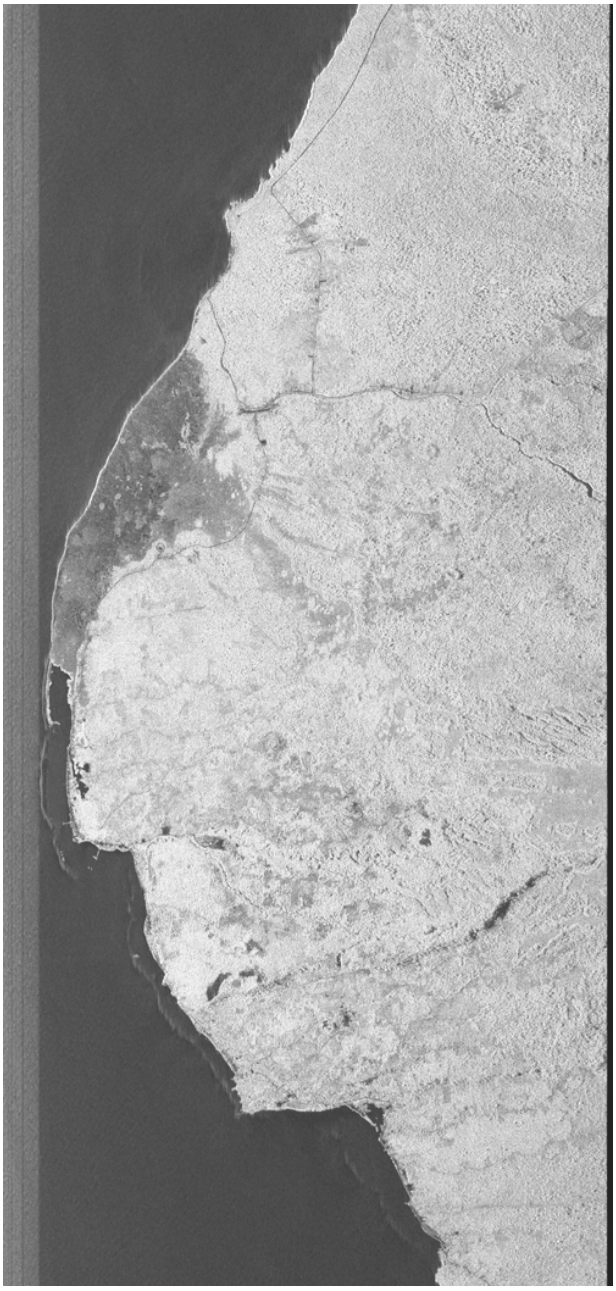

Figure 25: Example (Savaii293-1) where the cross-talk removal algorithm has obtained an incorrect result for the HV-pol scene in the near range due to low signal-to-noise. The failure is highlighted by the bright near-range (left side) streaking. The implication is that all of the signal over the ocean in the near range for the cross-pol channel is cross-talk noise. The cross-pol terms in the scattering matrix here are below the AIRSAR noise threshhold.

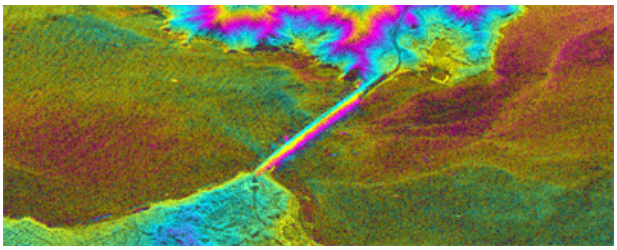

Figure 26: C-band along-track interferogram showing uncompensated phase signatures over significant relief.

a good choice for this reference elevation. However, many ATI scenes also have land in the scene. (In fact, land is helpful to obtain the absolute phase, or the absolute velocity offset.) The phase error introduced for scatterers located away from the elevation reference is given by:

$$\Delta\phi = \frac{4\pi b_z h}{\lambda r}, \tag{6}$$

where b_z is the vertical component of the baseline, h is the height difference between the scatterer and the elevation reference, λ is the wavelength, and r is the range to the scatterer.

This effect is illustrated in Figure 26, a C-band interferogram of San Francisco Bay showing the Golden Gate Bridge and the hills beyond. The topography in the hills is as much as a few hundred meters away from sea-level. For PacRim 2000, all ATI data were collected in the "common-transmitter" mode, i.e., always transmit aft, and receive both aft and forward antennas. For these data, using (6), a full 360 degrees of phase error occurs when the deviation of the topography from the elevation reference (sea-level) is:

C-band	800-1300 m
L-band	6600-10000 m

where no pitch has been assumed in the C-band case, while the L-band case corresponds to one degree of pitch. (b_z comes strictly from platform attitude in the case of L-band, while there is a "built-in" C-band vertical baseline in ATI mode.)

Although the topography is not compensated in the ATI processor, the effect on ocean scenes should be negligible. If (6) is used, assuming a 10 m significant wave-height, then the velocity error introduced due to the vertical component of the baseline is:

C-band	5–7 degrees
L-band	< 0.5 degree

These errors are similar in magnitude to the uncertainty in the ATI velocity measurement due to the signal-to-noise ratio of the system.

Name:	ATI Topography
Impact:	Negligible for ocean currents
Correction:	Not implemented
Occurrence:	ATI with targets at height far from reference
Reprocessing:	(N/A)

5 Summary and Outlook

We have described here most of the data problems which we observe in recent AIRSAR data sets, especially those collected during the PacRim 2000 mission. In most of these cases, there are signal-processing workarounds which allow us to process and deliver these data sets. However, ideally, we would like to address these data problems at the source. The following is a summary of the steps we are taking to address these data problems.

5.1 New Digital Chirp Generators

As mentioned in the previous section, errors in the timing of the chirp generation can be fatal to data acquisition. Therefore, immediately upon our return from the PacRim 2000 deployment, we began to build new digital chirp generators. These will have much cleaner timing distribution, which should prevent the kinds of errors we saw during PacRim 2000. The new DCG's are being used during the AirSci'02 data acquisition campaign. These have the added advantage that we have built extras, which can not only be used as "in-flight spares", but can be used to indepently

control all three (or more) radars, once the appropriate additional RF stage is built. This will allow us to use completely independent chirps for the three radars, for example, 80 MHz at L-band, 40 MHz at C-band, and 20 MHz at P-band. Currently, the C-band radar must be turned off when we transmit an 80 MHz chirp for the high-resolution L-band mode. Finally, the DGS's are VME-based, allowing us to further miniaturize the radar system. (The previous DCG's were rack-mounted.)

5.2 New Digital System

AIRSAR is building a new digital system in order to support the high-data rates desired for the Optical Communication experiment[9]. The higher data rates will also be a boon to AIRSAR investigators, since the current system is data-rate limited. Some of the current components of the AIRSAR digital system are over 15 years old; others which are newer were nevertheless uneasily integrated with the older components. The new system will be a coherent whole, including an integrated COTS ADC and data recording system. We anticipate that the "digital noise" described in this paper will be greatly reduced or eliminated with the advent of this new system.

5.3 New P-band Transmitter

Starting with the AirSci'02 data acquisition campaign (IceSAR), AIRSAR is deploying a new P-band transmitter. The radiated power in the new system is 3 dB more than that of the old. We anticipate that the combination of a significant increase in P-band signal-to-noise, combined with continued improvements in the RFI-rejection filtering[10] will reduce, though certainly not eliminate, the impact of RFI contamination of AIRSAR data.

5.4 Improved Motion Sensing

One of the operational difficulties during the PacRim 2000 mission was the embedded GPS-INU (EGI) which seemed to have trouble integrating the GPS and inertia data to produce accurate position and attitude information. After PacRim 2000 was concluded, Honeywell engineers uploaded a newer version of the EGI firmware. This may reduce some of the problems we experienced during the PacRim 2000 mission, and should reduce the geo-location errors we experienced for the PacRim 2000 data sets.

Improved accuracy GPS corrections are now being made available in real-time. The AIRSAR instrument has been outfitted to receive and record the improved-accuracy positions with a 12-channel Ashtec GPS receiver. These positions are integrated with the EGI position and attitude information in the AIRSAR processor, and should reduce the EGI position errors (15–30 m) substantially.

5.5 New Processing Technology

The processing technology developed[11] (and already partially implemented in the AIRSAR ATI processor[12]) recently will be incorporated into the AIRSAR integrated processor. The improved motion compensation, pulse-resampling and regridding schemes should help to reduce the motion-related artifacts and patch-boundaries described in this paper. Initially, the improved technology processor may only be available for TOPSAR DEM data (without co-registered polarimetry) which we concede is a limitation. We hope that this limitation will eventually be lifted.

Acknowledgement

The research described in this paper was carried out by the Jet Propulsion Laboratory, California Institute of Technology, under a contract with the National Aeronautics and Space Administration. Several members of the AIRSAR processing team have contributed both to the detection as well as to

[9] *Rapid-Response Disaster Management Demonstrations Using In-flight Laser Downlinks of AIRSAR Data: Current and Future Plans, by David Pieri, elsewhere in the proceedings of this workshop.*

[10] *RFI Removal from AIRSAR Polarimetric Data*, by Charles Le and Scott Hensley, elsewhere in the proceedings of this workshop.

[11] *Improved Processing for AIRSAR Data Based on the GeoSAR Processor*, by Scott Hensley, Elaine Chapin, and Thierry Michel, elsewhere in this workshop proceedings.

[12] *PacRim 2000 ATI Calibration*, by David A. Imel, elsewhere in this workshop proceedings.

the correction of the data problems described here. In particular, Yunling Lou has developed the CV-banding correction and Anhua Chu has developed many of the other processing workarounds described here.